Published in final edited form as:
Proteins. 2012 March ; 80(3): 935–945.

Identification of the bile salt binding site on IpaD from *Shigella flexneri* and the influence of ligand binding on IpaD structure

Michael L. Barta[1], **Manita Guragain**[2], **Philip Adam**[2], **Nicholas E. Dickenson**[2], **Mrinalini Patil**[2], **Brian V. Geisbrecht**[1], **Wendy L. Picking**[2], and **William D. Picking**[2,*]

[1]Division of Cell Biology, School of Biological Sciences, University of Missouri-Kansas City, Kansas City, MO

[2]Department of Microbiology and Molecular Genetics, Oklahoma State University, Stillwater, OK

Abstract

Type III secretion (TTS) is an essential virulence factor for *Shigella flexneri*, the causative agent of shigellosis. The *Shigella* TTS apparatus (TTSA) is an elegant nano-machine that is composed of a basal body, an external needle to deliver effectors into human cells, and a needle tip complex that controls secretion activation. IpaD is at the tip of the nascent TTSA needle where it controls the first step of TTS activation. The bile salt deoxycholate (DOC) binds to IpaD to induce recruitment of the translocator protein IpaB into the maturing tip complex. We recently used spectroscopic analyses to show that IpaD undergoes a structural rearrangement that accompanies binding to DOC. Here we report a crystal structure of IpaD with DOC bound and test the importance of the residues that make up the DOC binding pocket on IpaD function. IpaD binds DOC at the interface between helices α3 and α7, with concomitant movement in the orientation of helix α7 relative to its position in unbound IpaD. When the IpaD residues involved in DOC binding are mutated, some are found to lead to altered invasion and secretion phenotypes. These findings suggest that adoption of a DOC-bound structural state for IpaD primes the *Shigella* TTSA for contact with host cells. The data presented here and in the studies leading up to this work provide the foundation for developing a model of the first step in *Shigella* TTS activation.

Keywords

Shigella; dysentery; invasion plasmid antigens; invasion; bile salts

INTRODUCTION

Shigella flexneri is a Gram-negative, facultative intracellular bacterium that causes shigellosis, a severe form of human bacillary dysentery. Every year, 165 million cases of shigellosis occur worldwide with more than one million deaths [1]. The bacterium can be acquired from contaminated water or be spread by the fecal-oral route with as few as 10–100 organisms sufficient to cause disease [2]. A key step in the onset of shigellosis is bacterial invasion of colonic epithelial cells. The genes required for intestinal epithelial cell invasion are located on a 31-kb fragment of a large virulence plasmid which encodes a type III secretion system (TTSS) and numerous effector proteins [3].

TTSS are key virulence factors for many Gram-negative pathogens, and serve as a channel that directly connects the bacterium to the host cell. TTSS architecture resembles that of a

*Corresponding author: Department of Microbiology and Molecular Genetics, Oklahoma State University, 307 Life Sciences East, Stillwater, OK 74078, Tel. 405-744-6243, william.picking@okstate.edu.

molecular syringe containing a cytoplasmic bulb, a basal body that spans the inner and outer bacterial membranes and an external needle possessing a tip complex at its distal end [3–5]. The bacterial protein IpaD localizes at the needle tip of *S. flexneri* prior to secretion induction [6]. IpaD is a dumbbell shaped protein with a stabilizing intramolecular coiled-coil flanked by two globular domains; this protein is responsible for regulating secretion. The N-terminal two helix chaperone domain of IpaD has been proposed to prevent self-association prior to its secretion through the molecular syringe [7]. Meanwhile, the C-terminal domain is necessary for binding of IpaB following its recruitment to the needle tip [7]. IpaD recruits and stably associates with the first true translocator protein, IpaB, at the needle tip, in the presence of environmental stimuli like deoxycholate (DOC) and other bile salts [8]. This occurs with a concomitant increase in *Shigella*'s ability to invade cultured cells [4]. Computer docking simulations predicted, and fluorescence spectroscopy experiments confirmed that DOC can associate with IpaD, possibly within a cleft formed by the interface of the two helices (α3 and α7) that form the central coiled-coil [8].

Because IpaD can be detected at the TTSS needle tip prior to any other secreted proteins [6] and since bile salts lead to recruitment of IpaB to the IpaD/needle tip complex [9], we have proposed that IpaD serves as a small-molecule biosensor at the tip of the TTSA needle. It can thus trigger the recruitment of IpaB to form the needle/IpaD/IpaB ternary complex which is then primed for full TTS induction immediately upon detecting host cell contact. Furthermore, we recently suggested that IpaD undergoes a conformational change upon DOC binding [10]. To refine these findings so that a mechanism for TTSA priming can be developed, we have now determined a crystal structure of a large fragment of IpaD bound to DOC. This allows us to make the first structural comparison between the bound and free IpaD structures (PDB entries 2J0O and 2J0N) [7]. Significantly, this DOC-bound structure has identified a bile-salt binding site that differs from what was previously predicted [8]. Based on identification of the binding site reported here and knowing the structural adaptations that either allow or result from DOC binding, mutants were generated to better understand the role of DOC in initiating recruitment of IpaB to the TTSA needle tip and the influence of this event on *Shigella* invasion functions. Single point mutations in the newly identified DOC binding pocket were found to influence IpaD's ability to direct *Shigella* invasion of cultured cells, while elimination of the two residues that appear to strongly interact with DOC greatly reduced the ability of IpaD to direct invasion or control secretion. The overall findings appear to indicate that the binding of small molecules at the TTSA needle tip stabilizes an alternative conformation in IpaD that is ultimately sensed by the apparatus and which promotes a single, discrete step in TTS. This step occurs without inducing full TTS and appears to prime the system for making contact with a host cell.

MATERIALS AND METHODS

Materials

The *S. flexneri ipaD* null strain (SF622) was from P.J. Sansonetti (Institute Pasteur, Paris, France). Antibodies against IpaB, IpaC and IpaD were provided by E.V. Oaks (Walter Reed Army Institute for Research, Silver Spring MD). Alexa-fluor labeled secondary antibodies were from Invitrogen. *E. coli* Nova Blue cells and ligation reagents were from Novagen (Madison, WI). Restriction enzymes were from New England Biolabs (Tozer, MA). Oligonucleotide primers were from IDT (Coralville, IA). All other chemicals were reagent grade.

Bacterial strains

The strains used in this study are listed in Table I. All *ipaD* mutants were constructed by inverse PCR using pWPsf4D (which contains a copy of the wild-type *ipaD* gene [11]) as a

template and primers incorporating the desired mutation. The resulting linear plasmid was digested with *Nde*I, intramolecularly ligated, and introduced into *E. coli* Nova blue cells by transformation. Each plasmid was subsequently purified and introduced by electroporation into *S. flexneri* SF622. Ampicillin selection ensured the presence of the recombinant plasmid while kanamycin resistance and/or Congo red binding were used to ensure the presence of *S. flexneri* virulence plasmid.

Cloning, over-expression and purification of recombinant IpaD

A gene fragment encoding IpaD residues 39–322 (possessing a C322S mutation to prevent covalent dimerization) was amplified from the *S. flexneri* virulence plasmid using PCR and the resulting fragment was subcloned into the expression plasmid pT7HMT [12]. The sequence-confirmed plasmid was transformed into *Escherichia coli* BL21 (DE3) cells, which were then cultured in Terrific Broth supplemented with kanamycin (50 μg/ml) at 37 °C to an A_{600nm} of 0.8. Protein expression was induced overnight at 18 °C by adding IPTG to 1 mM. Bacterial cells were harvested by centrifugation, resuspended in lysis buffer (20 mM Tris (pH 8.0), 500 mM NaCl, and 10 mM imidazole), and then lysed by microfluidization. The soluble tagged protein was collected in the supernatant following centrifugation of the cell homogenate and purified on a Ni^{2+}-NTA Sepharose column according to published protocols [12]. Recombinant TEV protease was used to digest the fusion affinity tag from the target protein as previously described [12]. After desalting into 20 mM Tris (pH 8.0), final purification was achieved by Resource Q anion-exchange chromatography (GE Biosciences). Following this, the purified protein was concentrated to 30 mg/ml, buffer exchanged by ultrafiltration into double-deionized water, and stored at 4 °C for further use.

Crystallization

Whereas attempts to cocrystallize “full-length” IpaD (residues 39–332) in the presence of DOC failed to yield any samples suitable for X-ray diffraction analysis, unexpected in-drop proteolysis of IpaD in the presence of a molar excess of DOC (~0.3 mM) yielded single block-shaped crystals after 4 months at 20 °C. Optimization of the mother liquid condition resulted in the overnight formation of large, block-shaped crystals (~300 μm in diameter), which could be reproduced by vapor diffusion of hanging drops with the degraded $IpaD^{122.319}$ sample. In particular, 1 μl of protein solution (10 mg/ml in double-deionized water) was mixed with 1 μl of reservoir solution that contained 20 mM magnesium chloride hexahydrate, 100 mM HEPES (pH 7.5) and 20% (w/v) polyacrylic acid sodium salt 5100, and equilibrated over 500 μl of reservoir solution. Crystals were flash cooled in a cryoprotectant solution consisting of reservoir buffer with an additional 15% (v/v) glycerol.

Diffraction data collection, structure determination, refinement and analysis

Monochromatic X-ray diffraction data were collected at −173 °C to 1.9 Å limiting resolution from a single crystal using beamline 22-BM of the Advanced Photon Source, Argonne National Laboratory (Table II). Following data collection, individual reflections were indexed, integrated and merged using HKL2000 [13]. Initial phase information was obtained by maximum-likelihood molecular replacement using PHASER [14]. Specifically, chain A of PDB entry 2J0O (wild-type *S. flexneri* IpaD) was manually truncated to residues 131–322 within PyMol [15] to reflect the truncated form of IpaD within the cocrystal, and this resulting structure was used as a search model. The single most highly scored solution contained an IpaD dimer in the asymmetric unit; this arrangement corresponded to a Matthews coefficient of 2.93 $Å^3$/Da and a solvent content of 57.7%.

Structure refinement was carried out using the protocols implemented in *phenix. refine* [16]. To begin, one round of simulated annealing, individual coordinate and isotropic atomic-

displacement factor refinement was conducted, and the refined model was used to calculate both $2F_o-F_c$ and F_o-F_c difference maps. These maps were used to iteratively improve the model by manual building in Coot [17,18], followed by additional coordinate and atomic-displacement factor refinement. Ordered solvent molecules were added according to the default criteria of *phenix. refine*, and inspected manually using Coot prior to model completion. Additional information and refinement statistics are presented in Table II. Chain A contains an intact polypeptide encompassing residues 122–319, while regions of poor map quality corresponding to residues 174–194 and 270–278 prevented complete sequence coverage for chain B.

Ligand fitting

Inspection of the initial F_o-F_c difference maps described above revealed unmodeled contiguous density that corresponded to DOC bound in a region near the N-termini (α3 and α7) of both polypeptides within the asymmetric unit. To appropriately model this ligand, a PDB file for DOC was first prepared using the PRODRG server [19], and molecular restraint files were generated using *phenix. elbow* [16]. Then *phenix. ligandfit* [16] was used to place a single DOC molecule per IpaD monomer. Refinement of the ligand-bound IpaD structure was carried out as described above, with the exception that constrained group occupancy refinement was used to estimate the fraction of ligand bound at each site independently.

Overnight Ipa protein secretion

Shigella were grown overnight at 37°C with aeration in tryptic soy broth (TSB). The bacteria were then removed by centrifugation at 6000 × *g* and the proteins in the culture supernatant were precipitated by bringing the solution to 10% (w/v) with trichloroacetic acid and incubating at 4°C. The precipitated protein was collected by centrifugation at 10,000 × *g* for 10 min and the resulting pellet washed with ice-cold acetone prior to resuspending in 10mM sodium phosphate (pH 7.2) containing 150mM NaCl (PBS). Two volumes of SDS-sample buffer were then added and the proteins were separated by SDS-polyacrylamide gel electrophoresis (SDS-PAGE). The proteins were then transferred to nitrocellulose for routine immunoblot analysis using a mixture of antibodies against IpaB, IpaC, and IpaD. Proteins were detected using Alexa Fluor 680-labeled goat anti-rabbit IgG. Western blot images were obtained using an Odyssey Infrared Imaging System (LI-COR, Lincoln, NE).

Bacterial invasion of cultured epithelial cells and contact-mediated hemolysis

S. flexneri invasion of HeLa cells was monitored with a gentamycin protection assay as previously described [11]. HeLa cells were seeded into 24-well plates and grown overnight in MEM supplemented with 10% calf serum (containing penicillin and streptomycin) at 37 °C, 5% (v/v) CO_2, and a relative humidity of 100%. *S. flexneri* was then grown on trypic soy agar plates containing 0.025% (w/v) Congo red. Ampicillin was included on plates for growing bacteria harboring pWPsf4 to maintain the plasmid. Red colonies (indicative of bacteria that had not lost the *Shigella* virulence plasmid) were used to inoculate 10 ml of TSB containing kanamycin (to maintain the virulence plasmid if the bacteria were derived from SF622) and ampicillin (to ensure maintenance of the pWPsf4 plasmid). The bacteria were grown at 37°C to early log phase (A_{600} ~ 0.4) with aeration. The cultures were then split so that half could be incubated for the final 30 min in the presence of 2.5 mM (0.1% w/v) deoxycholate (DOC). The bacteria were then incubated with the HeLa cells for 30 min as described [11] without the centrifugation step. Extracellular bacteria were killed with 50 μg/ml gentamycin. The invading bacteria were visualized by overlaying the HeLa cell monolayers with 1.0% agarose in water, followed by an overlay of 2× LB media in agar. After overnight incubation at 37 °C, the colonies were counted and the relative level of invasion for bacteria

making mutant IpaD was compared to that of *S. flexneri* SF622 harboring pWPsf4D which expressed wild-type IpaD.

Shigella contact-mediated hemolysis was initially measured as described previously [11]. Because this method essentially results in 100% lysis of the erythrocytes, it was modified by reducing the number of bacteria incubated with the epithelial cells and shortening the incubation time. This allowed us to obtain subsaturating levels of contact-mediated hemolysis which could be used to detect subtle differences caused by *Shigella* expressing different mutant forms of IpaD. Briefly, bacteria were grown to mid-log phase, collected by centrifugation and resuspended in PBS. Sheep red blood cells were washed and resuspended in PBS to a concentration of 10^{10}/ml. Blood cells and bacteria were mixed and forced into contact by centrifuging at 2,200 × *g* for 15 min at 20°C. The cells were then incubated at 37°C for 30 min, resuspended in cold PBS and centrifuged again at 2,200 × g. The amount of hemolysis was then measured by determining the absorbance of the resulting supernatant fraction at 545 nm. The data are presented as a percent of total lysis, which was determined by incubating the erythrocytes in water. Incubation in PBS served as a negative control for hemolysis.

Surface localization of IpaD

To visualize the presence of IpaD at the tip of the *S. flexneri* TTSA needle, bacteria were first grown to early log phase (A_{600} ~0.4) in TSB with or without 2.5 mM DOC. The bacteria were then collected by centrifugation, resuspended in PBS, and fixed with 1.5% (v/v) formaldehyde. The bacteria were affixed to glass slides and blocked with 1% (w/v) bovine serum albumin in PBS:Odyssey blocking buffer (1:1) (LiCor Biosciences, Lincoln, NE). IpaD was detected using rabbit anti-IpaD antiserum as the primary antibody and Alexa Fluor 488 goat anti-rabbit IgG as the secondary antibody. Fluorescence microscopy was the carried out using an Olympus IX-81 spinning disk confocal microscope using a mercury light source with the appropriate bandpass filters to excite the fluorophore. In multiple fields ($n \geq 10$), the number of bacteria with IpaD on their surface was determined as a function of total bacteria in the field. In some cases where the bacteria were found to have elevated invasion levels in the absence of DOC, they were examined for the presence of IpaB on their surfaces prior to DOC-induced maturation.

RESULTS

Structure of the IpaD$^{122.319}$-DOC complex

IpaD$^{122.319}$-DOC cocrystals were generated as described in Methods and diffracted synchrotron X-rays to 1.9 Å limiting resolution. Since the initial crystals took nearly 4 months to appear, a number of routine analyses were conducted to address potential questions regarding sample degradation. In particular, the results of SDS-PAGE and MALDI-TOF strongly suggested proteolytic loss of α helices 1–2′ (approximately residues 40–120) that comprise the IpaD N-terminal domain. With this information, the crystal structure was then solved by molecular replacement and contained two molecules of IpaD$^{122.319}$ within the asymmetric unit (Supplemental Figure S1). Significantly, F_o–F_c maps (calculated as described in Methods) revealed unmodeled contiguous density (Fig. 1A, following refinement and Supplemental Figure S2, prior to refinement) that represented a single copy of bound DOC near the N-terminus (α3 and α7) of each IpaD$^{122.319}$ polypeptide. Upon placing each DOC ligand, the final model was refined to R_{work} and R_{free} values of 22.9% and 25.5%, respectively (Fig. 1B and Table I).

In light of previous findings [8], the more relevant 1:1 complex was that shown in Figure 1C in which DOC is bound by a hydrophobic pocket formed by the interface of α3 and α7 of

the central IpaD$^{122.319}$ coiled-coil. While this was lower on the coiled-coil than predicted by previous computer docking simulations, it was still consistent with Förster resonance energy transfer (FRET) measurements between a coumarin fluorescence donor probe on Cys322 and the fluorescein acceptor tethered via a linker on FITC-DOC [8] when the length of the linker and dimensions of FITC were considered. The FRET-based distance between these two probes was determined at 42 Å and this was originally interpreted to position the DOC binding site about half way up the central coiled-coil of IpaD$^{122.319}$. However, when the length of the six-carbon tether linking the fluorescein (~20 Å) to DOC is considered, the FRET measurements are still in agreement with the Cys322-DOC distance measured in the crystal, and would actually be expected to lie in approximately the position shown in Figure 1C.

When the structure of IpaD$^{122.319}$ with DOC bound was superimposed with free structures of IpaD ("full-length", 2J0O and truncated, 2J0N), it was apparent that bile salt binding was accompanied by a change in the overall conformation of the protein (Fig. 2A). However, structural superposition of DOC-bound IpaD with free, truncated IpaD (Figure 3) reveals that DOC interaction stabilizes a pre-existing intrinsic conformation within IpaD. Specifically, the central coiled-coil (α3 and α7) became constricted by 2.7 Å in the DOC-bound state, with α5 of the C-terminal domain contracting slightly as well. This constriction of α7 led to a 7.8 Å shift with respect to its original position within free IpaD. Again, however, these data were consistent with the previous FRET-based findings of Dickenson *et al.* [10] who proposed that a kink formed between residues 146 and 149 in α3 of the central coiled-coil may be a key contributor to the conformational changes observed in solution. This change is illustrated in the structural overlay depicted in Figure 2B. It was previously found that DOC binding to an N146Q mutant of IpaD did not appreciably change the conformational distribution of the protein between free and bound states (as determined by NMR chemical shift mapping) [10]. This was accompanied by a significant reduction in *Shigella* invasiveness. Interestingly, while Dickenson *et al.* [10] proposed that DOC binding likely stabilized the helical character of α3, the overlay in Figure 2B instead suggests that ligand binding stabilizes formation of a bulge at this position.

Site directed mutagenesis of residues involved in DOC binding – effect on host cell invasion

The IpaD$^{122.319}$-DOC structure described in Figure 1 was analyzed by the CCP4 program *Contact* [20,21] to identify residues located within 2.6 – 5.0 Å of DOC that appeared to contribute to DOC binding. This identified several positions along IpaD helix α3 (Ile129, Lys137, Ile138, Ser141 and Ile145) as well as a single residue (Leu311) along helix α7, however, two other residues within this hydrophobic pocket appeared to be most intimately involved in DOC binding. These two residues were Leu134 and Leu315, which are highlighted within Figure 4. Using this information, a majority of these positions were targeted for mutagenesis to directly assess their importance with respect to DOC binding and IpaD function. In particular, changes to serine were used to render these normally hydrophobic positions more polar, while changes to glutamate were used to introduce a formal negative charge at these sites.

Whereas several mutants displayed invasion phenotypes that were largely similar to that of *S. flexneri* SF622 expressing wild-type IpaD (the results for only K137S and I138S are shown in Table III), two of the mutants proposed to be most directly involved in DOC binding showed notable changes in invasiveness (Table III). In a typical experiment, the addition of DOC has been shown to cause a three- to four-fold increase in *Shigella* invasiveness of cultured HeLa cells [9]. Significantly, the L134S and L134E mutants displayed enhanced invasiveness relative to wild-type IpaD in the absence of DOC. The

addition of DOC then had what appeared to be a reduced stimulatory effect on this level of invasiveness (Table III). L315S was also mildly enhanced in invasiveness relative to wild-type IpaD, however, and the addition of DOC to *Shigella* expressing this mutant caused an increase in invasiveness that was somewhat greater than expected (approaching six-fold; Table III). Together, these findings suggested that L134 and L315 contribute in important ways to the observed DOC effect on *Shigella* invasiveness.

In contrast to what was seen with the mutations L134S, L134E or L315S, mutation of L315 to glutamate (L315E) resulted in a nearly complete loss of invasiveness (Table III). A similar phenotype was observed if L134 and L315 were mutated simultaneously to serine or glutamate (L134S/L315S and L134E/L315E, respectively) (Table III). Because the latter mutants contained multiple mutations, it was possible that their loss of function was due to induced structural instability, however, each protein could be purified without observable degradation and their circular dichroism (CD) spectra were nearly identical to free IpaD.

Because some of the mutations at L134 and L315 resulted in what appeared to be enhanced invasiveness prior to DOC addition, it was also possible that they might be causing IpaB to appear prematurely on the bacterial surface. Indeed, this appeared to be the case since immunofluorescence microscopy showed staining for IpaB on the surface of *S. flexneri* even in the absence of DOC (approximately 93% of cells in each case). At the same time, the same sets of mutations did not change the levels of IpaD presentation on the *Shigella* surface relative to bacterial expressing wild-type IpaD (Table III). Thus, when considered as a whole, these results suggest that L134 and L315 of IpaD have important roles in invasion by *S. flexneri*.

Effect of mutations on contact-mediated hemolysis by *Shigella*

Contact hemolysis provides a measure of *Shigella*'s ability to insert translocon pores into target cells when the two are forced into contact with one another. As such, it provides an alternative measure of TTSA maturation and function. When the standard contact-mediated hemolysis assay was modified so that it gave a subsaturating level of erythrocyte lysis, similar trends were observed as for the invasion results presented above in the absence of DOC (Table III). *S. flexneri* producing mutant forms of IpaD that had lost their invasion ability (notably L315E, L134S/L315S and L134E/L315E) were unable to cause significant red blood cell lysis, which indicated that they could not efficiently insert a functional translocon pore into the erythrocytes [22]. L315E did appear to display a minor amount of contact hemolytic activity that seemed to correlate with its very low level of invasiveness. Interestingly, those mutants that displayed elevated invasiveness relative to *S. flexneri* making wild-type IpaD in the absence of DOC also appeared to demonstrate modest increases in contact hemolysis activity (Table III).

In contrast to the invasion results following the addition of DOC, there was no clear increase in contact hemolysis by bacteria following incubation with DOC. In fact, *Shigella* making wild-type IpaD appeared to show a decrease in contact hemolysis activity (Table III). This is probably due to the fact that this assay requires that the bacteria be forced into contact with the red blood cells, thereby making it inherently less sensitive to any subtle changes that might be caused by prior incubation with DOC. Nevertheless, mutations within the DOC binding pocket of IpaD did appear to influence *Shigella's* contact hemolysis activity; however, monitoring invasion appears to be the most sensitive method to follow the TTSA needle tip maturation process.

The ability to properly deliver a functional translocon pore (consisting of IpaB and IpaC) into target cells is essential for delivery of the effector proteins needed for cellular invasion. Because of this, one possible reason for the inability to invade or cause contact-mediated

hemolysis was that the IpaD mutants had lost the ability to remain stably anchored at the TTSA needle tip. Indeed, this appeared to be the case as judged by immunofluorescence microscopy studies. While *S. flexneri* producing mutant forms of IpaD that could not restore invasion or contact-hemolysis failed to show detectable staining for IpaD on their surfaces in the presence or absence of DOC (Table III), all of the invasive *Shigella* strains showed similarly high levels of IpaD on their surfaces without regard to DOC. Curiously, L315E displayed very low levels of both invasiveness and contact hemolysis and had variable staining for low levels of IpaD on the surface (Table III), however, DOC addition for this mutant resulted in loss of invasiveness, contact hemolysis, and IpaD surface localization altogether.

Influence of IpaD mutations on secretion control

As mentioned above, the loss of invasiveness for L134S/L315S correlated with a loss of detection of IpaD on the *Shigella* surface (Table III). Because an important function of IpaD is to control type III secretion, the different IpaD mutants were likewise examined with respect to overnight secretion of the translocators. As would be expected, an *ipaD* null strain (SF622) showed no IpaD in overnight culture supernatant fractions, but released elevated levels of IpaB and IpaC into the medium. This reflected an inherent inability to control background levels of type III secretion; however, secretion control was restored back to low overnight levels when SF622 was complemented with wild-type IpaD (Fig. 5). This level of secretion control was equivalent to what has been seen routinely for both complemented and wild-type *S. flexneri* [11].

For most of the remaining IpaD single-site mutants described in Table III, overnight secretion appeared to be approximately equivalent to that of the wild-type form of the protein. In contrast, the L134S/L315S double mutant had completely lost secretion control and released amounts of IpaD, IpaB and IpaC into *Shigella* culture supernatant fractions that were even greater than that seen for the *ipaD* null mutant (Fig. 5). The L134E/L315E and L315E mutants gave similar results (data not shown). Based on surface localization experiments (Table III), there could be a change in their conformational distribution that leads to a disruption of the protein-protein contacts needed to maintain IpaD at the TTSA needle tip. In this regard, it is interesting to note that a similar phenotype was observed for IpaD when short C-terminal deletions had been introduced [11]. In these deletion mutants, IpaD retained its structural integrity, but was released into the culture supernatants along with IpaB and IpaC at greatly elevated levels.

DISCUSSION

In this report, we have expanded upon previous studies [10] by generating *Shigella* strains that express mutant forms of IpaD and performing detailed phenotypic analyses of the earliest stages of TTSA needle-tip complex formation and progression. This work was made possible by identifying a bile salt-binding pocket in IpaD, as judged by a 1.9 Å cocrystal structure of DOC bound to a core fragment of IpaD (i.e. IpaD$^{122.319}$). Even though initial crystallization studies were conducted with “full-length” protein, time-dependent proteolytic degradation of IpaD occurred slowly in the presence of saturating levels of DOC and lead to the loss of helices 1 to 2′ specifically (approximately up to residue 120). These residues comprise a small domain that has previously been proposed to serve a self-chaperoning function that prevents premature IpaD oligomerization [7]. A similar, yet even more extensively truncated form of IpaD (i.e. residues 133–319; PDB ID 2J0N) was also identified during the prior crystallographic studies of Johnson *et al.* [7]. Indeed, superposition of this truncated form of IpaD with that of DOC-bound IpaD reveals that both polypeptides adopt similar structures (168/198 Cα positions align within 5.0 Å with an RMSD of 1.18 Å,

Figure 3). It is interesting to note while that the truncated IpaD characterized by Johnson *et al.* was generated by an unknown protease during crystallization trials over a period of up to 12 months [7], the degradation product described here arose in the presence of DOC over a 4 month period. Furthermore, the extent of degradation within the DOC-bound structure was significantly less, as a minimum of 11 N-terminal amino acids (residues 122–143 within chain A and 122–132 within chain B) were degraded away in the free, truncated IpaD structure (Figure 3). It is possible that DOC binding stabilizes this region of IpaD in the absence of the N-terminal chaperone domain, as DOC binding is intimately associated with this region of IpaD (Figure 4). Finally, loss of the self-chaperone domain in IpaD was both time and DOC-dependent, since "full-length" IpaD itself is stable up to one year at concentrations approaching 1 mM in neutrally-buffered saline solutions (unpublished observations).

Protease sensitivity in the presence of ligand(s) has been documented in the past, and has found use as a sensitive biochemical probe for changes in protein conformation and dynamics [23]. For example, increased trypsin sensitivity in the presence of a small bacterial protein (~8.5 kDa) was used to identify a conformational change in the human complement protein C3b (~175 kDa) [24,25]. Such changes in C3b involve fairly substantial movements while the conformational differences seen for free and DOC-bound IpaD appear to be less dramatic. In particular, the IpaD structural differences are centered around exacerbation of the helical bulge in α3 and a constriction of the central α3–α7 coiled-coil of IpaD (Fig. 2A,B). It has to be noted that loss of the self-chaperone domain when preparing the crystals used for determining the structure presented here precludes a comparison between free and DOC-bound forms for the "full-length" IpaD. The absence of the N-terminal chaperone domain from the DOC-bound structure may, however, actually provide a more appropriate protein model with respect to IpaD structure. The chaperone domain of IpaD is proposed to move away from the protein body (*i.e.* the central coiled-coil) as it docks at the needle tip [6,7,22]. Because of such structural flexibility in IpaD, recent models of ligand-mediated structural transitions would argue that DOC binding actually stabilizes a pre-existing intrinsic conformation in IpaD, rather than "inducing" an altogether new conformation *per se* [26,27]. Thus, the truncated form of IpaD identified by Johnson *et al.* may actually represent the ligand-bound conformation of IpaD seen in the absence of DOC. Finally, while it would be overly speculative to comment on the statistical distribution between the free and DOC binding-competent forms within "full-length" IpaD, the fact that conformational changes could be detected by both FRET and NMR shift mapping in the presence of DOC strongly suggest that these transitions must occur readily, at least *in vitro*.

Mutational analysis presented here reveals that disruption of the two IpaD residues most closely linked to DOC binding (L134 and L315) resulted in the greatest effects on IpaD's role as a virulence factor. In particular, both the L134S/L315S and L315E mutants lost control of secretion regulation, which potentially implicates the ability to bind DOC in maintenance of IpaD at the needle tip. Since DOC-binding correlates with structural differences in IpaD (as determined by FRET, NMR, and now crystallography), it is possible that changes emanating from the DOC binding pocket precipitate minor conformational shifts that affect the manner in which IpaD interacts with the TTSA needle. In the most conceptually-simple case, mutations that influence these conformational changes could impact how well IpaD is stably maintained at the TTSA needle tip. This would be interesting because loss of IpaD from the bacterial surface following mutation of residues within its DOC-binding site suggests that bile salts influence key protein-protein interactions within the needle tip complex and, further, that these interactions are critical for regulating secretion control. It is also possible that these altered interactions could serve to propagate a DOC-mediated signal from the TTSA needle tip to the base of the TTSA structure. Finally, DOC binding could influence the nature of IpaD's interaction with the first translocator,

IpaB, which is held within the lumen of the TTSA needle or needle tip complex [9]. This could explain why only IpaB is recruited to the TTSA needle tip after following IpaD/DOC binding [9].

Recently there have been two papers published that describe the structures of the IpaD homologue from *Salmonella*, SipD, with bile salts bound. In the first of these, Chatterjee *et al.* presented the structures of a fragment of SipD ($SipD^{39.342}$) bound to deoxycholate and chenodeoxycholate [28]. Comparison of these structures with that of $IpaD^{122.319}$-DOC described here reveals two noteworthy differences. First, while DOC binding appears to involve an alternative conformation in IpaD, indeed one that was additionally seen within PDB code 2J0N (Figure 3) at a further truncated level, the apo-and bile salt-bound structures of $SipD^{39.342}$ are nearly identical to each other [29]. Whether or not this is due to the presence of the N-terminal self-chaperone domain in SipD remains unclear at this time. Second, whereas the stoichiometry of the $IpaD^{122.319}$-DOC interaction presented here appears to be 1:1 for each IpaD monomer, the $SipD^{39.342}$ co-crystal structures displayed 1:1 stoichiometry only when considered within the context of the needle tip multimer [7]. Confounding the interpretation of these SipD data is a second paper, which was published after the present work was first submitted. In this report, Lunelli *et al.* proposed a DOC binding site on SipD that is entirely different than that described by Chatterjee and colleagues [30]. In particular, they analyzed a form of SipD fused to the *Salmonella* TTSA needle protein monomer PrgI, and suggested that DOC binding involved a region that arose via the interface of SipD and PrgI. Mutagenesis of the SipD residues involved in PrgI binding indicated that the residues involved in binding DOC were also important for SipD function. Among these positions in SipD are R232, Q233 and S236, which are in close proximity to the DOC binding site, as are at least eight residues from PrgI. This stands in perplexing contrast to the previous report on SipD [28], in which residues near the bile salt-binding site are derived from the two different polypeptides (i.e. R41, I45, K338 and F340 from the A subunit, and N104, A108, L318, N321 and L322 from the B subunit). In light of our work described here, it is actually this latter SipD binding site that corresponds more closely to the DOC-binding residues from IpaD. Nevertheless, it has to be mentioned that this binding site described by Chatterjee *et al.* is comprised of an interface between adjacent SipD monomers and involves residue contributions from the N-terminal chaperone domain, which is missing in the $IpaD^{122.319}$-DOC co-crystal.

When viewed at first glance, it would be tempting to speculate that the ligand-binding mode identified for IpaD is more relevant because it is supported by a previous series of *in vitro* binding studies [8]. It is critical to realize, however, that *Salmonella* respond much differently to bile salts than do *Shigella* [31]. Chief amongst these differences are that bile salts mediate repression of expression of *Salmonella* pathogenicity island 1 (SPI-1) which encodes the TTSS that includes SipD and PrgI (i.e. the needle protein) [32] and that short incubation in presence of DOC causes rapid loss of *Salmonella* invasiveness for cultured cells (unpublished results). Curiously, there exists a high degree of structural conservation between both the tip proteins (IpaD and SipD) [7] and the needle proteins (MxiH and PrgI) [32,33] from these two organisms. This suggests that the needle-tip protein interaction is likely to be conserved as well, even though the surface electrostatic features of MxiH and PrgI differ significantly. Thus, while it cannot be ruled out whether different electrostatic properties play a role, it is reasonable to suggest that the difference in binding modes presented here might ultimately give rise to pathogen-specific responses to the same bile salts. In any case, it is clear that fundamental differences in TTSA function exist between these two closely related organisms. Thus, additional work will be needed to dissect the molecular level changes that occur in response to bile-salts by other TTSAs [28].

As discussed earlier, the N-terminal domain of IpaD is predicted to swing away from the core of the protein upon association with MxiH at the needle tip. In line with this, the N-terminal portion of DOC-bound IpaD$^{122.319}$ assumes a non-canonical secondary structure that extends further away from the central α3–α7 coiled-coil than the same region within free IpaD$^{122.319}$ (Fig. 2C). Previously, Zhang *et al.* proposed a model of the IpaD-MxiH interaction in which α3 of IpaD plays a critical role [22]. Modeling of this interaction (Supplemental Figure S3) may place the C-terminal domain of IpaD on the outside of the needle core. More significantly in terms of the present work, it places the location of the DOC binding site identified here on the outside face of the needle. While there is currently some uncertainty regarding the number of IpaD molecules present in the tip complex, it seems fairly likely that the polypeptides involved in forming the secretion plug would continue the helical rise seen within the polymerization of the needle protein MxiH [7]. Thus, constriction of both helices comprising the central coiled-coil (as judged by the free versus DOC-bound IpaD structures) provides a potentially attractive mechanism for the opening of the needle pore. Anchoring of IpaD to MxiH would imply that a global constriction of the tip protein should pull IpaD away from the central pore of the needle. This scenario would resemble the opening of an iris on a microscope.

Our previous use of solution dynamics along with the crystalline state studies presented here have allowed for a comprehensive analysis of IpaD structural changes that correlate with its binding to bile salts. This has permitted well-informed mutagenesis and phenotypic analysis of what appears to be the first discrete step in TTS activation in *Shigella*, and also provided a framework for developing a testable model of this critical process. This initial step is characterized by the recruitment and stable binding of the first translocator protein, IpaB, to the maturing TTSA needle tip complex. At the tip of the nascent TTSA needle, IpaD is able to sense environmental small molecules such as bile salts that associate with the protein and thereby bind to the needle. The resulting stabilization of a particular IpaD conformation perturbs or alters the interaction between the tip complex and the needle itself, giving rise to a conformational signal that brings IpaB to the tip without further type III secretion. How this signal is processed by the apparatus is not clear; however, it could involve interactions between IpaD and IpaB, which is itself located within the needle prior to recruitment [9]. This would fit with the previous observation that while we do not detect IpaB on the surface of *S. flexneri* SF622 expressing wild-type IpaD, we can detect it by immunoblot analysis of isolated needles. Alternatively, it is possible that the DOC-stabilized structural transition at the needle tip is relayed through the polymerized needle monomers and then detected by the TTSA base. This would be consistent with previous studies which showed that point mutations within MxiH can lead to altered secretion status [34]. While there are still unanswered questions, this report provides a sound starting point for determining the mechanism of type III secretion induction in *Shigella*.

Supplementary Material

Refer to Web version on PubMed Central for supplementary material.

Acknowledgments

We gratefully acknowledge technical assistance from Daniel R. Picking and critical discussions with Chelsea R. Epler. This work was supported through funding from the NIH (R01 AI067858 to WLP, R21 AI090149 to WDP and F32 AI084203 to NED). Additional support was provided by the Oklahoma Health Research Program Funding (HR10-128S). The authors acknowledge generous technical assistance of Drs. Rod Salazar and Andy Howard during X-ray diffraction data collection. Use of the Advanced Photon Source was supported by the U. S. Department of Energy, Office of Science, Office of Basic Energy Sciences, under Contract No. W-31-109-Eng-38. Data were collected at Southeast Regional Collaborative Access Team (SER-CAT) beamlines at the Advanced Photon Source, Argonne National Laboratory. A list of supporting member institutions may be found at www.ser-cat.org/members.html

Abbreviations

Ipa	invasion plasmid antigen
Sip	*Salmonella* invasion protein
Mxi	major exporter of Ipas
PrgI	needle protein monomer from *Salmonella*
DOC	deoxycholate
TTS	type III secretion
TTSS	type III secretion system
TTSA	type III secretion apparatus
PBS	phosphate-buffered saline
TSB	trypticase soy broth
FRET	Forster resonance energy transfer
CD spectroscopy	circular dichroism spectroscopy

References

1. Diarrheal Diseases: Shigellosis. Volume 2009. World Health Organization; 2009. http://www.who.int/vaccine_research/diseases/diarrhoeal/en/index6.html
2. Niyogi SK. Shigellosis. J Microbiol. 2005; 43(2):133–143. [PubMed: 15880088]
3. Schroeder G, Hilbi H. Molecular pathogenesis of Shigella spp: controlling host cell signaling, invasion, and death by type III secretion. Clin Microbiol Rev. 2008; 21(1):134–156. [PubMed: 18202440]
4. Epler CR, Dickenson NE, Olive AJ, Picking WL, Picking WD. Liposomes recruit IpaC to the Shigella flexneri type III secretion apparatus needle as a final step in secretion induction. Infect Immun. 2009; 77(7):2754–2761. [PubMed: 19433542]
5. Mueller C, Broz P, Cornelis G. The type III secretion system tip complex and translocon. Mol Microbiol. 2008; 68(5):1085–1095. [PubMed: 18430138]
6. Espina M, Olive AJ, Kenjale R, Moore DS, Ausar SF, Kaminski RW, Oaks EV, Middaugh CR, Picking WD, Picking WL. IpaD localizes to the tip of the type III secretion system needle of Shigella flexneri. Infect Immun. 2006; 74(8):4391–4400. [PubMed: 16861624]
7. Johnson S, Roversi P, Espina M, Olive A, Deane JE, Birket S, Field T, Picking WD, Blocker AJ, Galyov EE, Picking WL, Lea SM. Self-chaperoning of the type III secretion system needle tip proteins IpaD and BipD. J Biol Chem. 2007; 282(6):4035–4044. [PubMed: 17077085]
8. Stensrud KF, Adam PR, La Mar CD, Olive AJ, Lushington GH, Sudharsan R, Shelton NL, Givens RS, Picking WL, Picking WD. Deoxycholate interacts with IpaD of Shigella flexneri in inducing the recruitment of IpaB to the type III secretion apparatus needle tip. J Biol Chem. 2008; 283(27):18646–18654. [PubMed: 18450744]
9. Olive AJ, Kenjale R, Espina M, Moore DS, Picking WL, Picking WD. Bile salts stimulate recruitment of IpaB to the Shigella flexneri surface, where it colocalizes with IpaD at the tip of the type III secretion needle. Infect Immun. 2007; 75(5):2626–2629. [PubMed: 17296762]
10. Dickenson NE, Zhang L, Epler CR, Adam PR, Picking WL, Picking WD. Conformational Changes in IpaD from Shigella flexneri upon Binding Bile Salts Provide Insight into the Second Step of Type III Secretion. Biochemistry. 2010
11. Picking WL, Nishioka H, Hearn PD, Baxter MA, Harrington AT, Blocker A, Picking WD. IpaD of Shigella flexneri is independently required for regulation of Ipa protein secretion and efficient insertion of IpaB and IpaC into host membranes. Infect Immun. 2005; 73(3):1432–1440. [PubMed: 15731041]

12. Geisbrecht B, Bouyain S, Pop M. An optimized system for expression and purification of secreted bacterial proteins. Protein Expr Purif. 2006; 46(1):23–32. [PubMed: 16260150]
13. Otwinowski, ZaMW. Processing of X-ray Diffraction Data Collected in Oscillation Mode. Methods in Enzymology. 1997; 276:307–326.
14. McCoy A, Grosse-Kunstleve R, Storoni L, Read R. Likelihood-enhanced fast translation functions. Acta Crystallogr D Biol Crystallogr. 2005; 61(Pt 4):458–464. [PubMed: 15805601]
15. DeLano, WL. The PyMOL Molecular Graphics System 2002. 2009. http://www.pymol.org
16. Adams P, Grosse-Kunstleve R, Hung L, Ioerger T, McCoy A, Moriarty N, Read R, Sacchettini J, Sauter N, Terwilliger T. PHENIX: building new software for automated crystallographic structure determination. Acta Crystallogr D Biol Crystallogr. 2002; 58(Pt 11):1948–1954. [PubMed: 12393927]
17. Emsley P, Cowtan K. Coot: model-building tools for molecular graphics. Acta Crystallogr D Biol Crystallogr. 2004; 60(Pt 12 Pt 1):2126–2132. [PubMed: 15572765]
18. Emsley P, Lohkamp B, Scott WG, Cowtan K. Features and development of Coot. Acta Crystallogr D Biol Crystallogr. 2010; 66(Pt 4):486–501. [PubMed: 20383002]
19. Schüttelkopf AW, van Aalten DM. PRODRG: a tool for high-throughput crystallography of protein-ligand complexes. Acta Crystallogr D Biol Crystallogr. 2004; 60(Pt 8):1355–1363. [PubMed: 15272157]
20. Potterton E, Briggs P, Turkenburg M, Dodson E. A graphical user interface to the CCP4 program suite. Acta Crystallography. 2003; D59:1131–1137.
21. The CCP4 Suite: Programs for Protein Crystallography. Acta Crystallography. 1994; D50:760–763.
22. Zhang L, Wang Y, Olive AJ, Smith ND, Picking WD, De Guzman RN, Picking WL. Identification of the MxiH needle protein residues responsible for anchoring invasion plasmid antigen D to the type III secretion needle tip. J Biol Chem. 2007; 282(44):32144–32151. [PubMed: 17827155]
23. Spolaore B, Bermejo R, Zambonin M, Fontana A. Protein interactions leading to conformational changes monitored by limited proteolysis: apo form and fragments of horse cytochrome c. Biochemistry. 2001; 40(32):9460–9468. [PubMed: 11583145]
24. Hammel M, Sfyroera G, Ricklin D, Magotti P, Lambris JD, Geisbrecht BV. A structural basis for complement inhibition by Staphylococcus aureus. Nat Immunol. 2007; 8(4):430–437. [PubMed: 17351618]
25. Chen H, Ricklin D, Hammel M, Garcia BL, McWhorter WJ, Sfyroera G, Wu YQ, Tzekou A, Li S, Geisbrecht BV, Woods VL, Lambris JD. Allosteric inhibition of complement function by a staphylococcal immune evasion protein. Proc Natl Acad Sci U S A. 2010; 107(41):17621–17626. [PubMed: 20876141]
26. Tsai CJ, Del Sol A, Nussinov R. Protein allostery, signal transmission and dynamics: a classification scheme of allosteric mechanisms. Mol Biosyst. 2009; 5(3):207–216. [PubMed: 19225609]
27. del Sol A, Tsai CJ, Ma B, Nussinov R. The origin of allosteric functional modulation: multiple pre-existing pathways. Structure. 2009; 17(8):1042–1050. [PubMed: 19679084]
28. Chatterjee S, Zhong D, Nordhues BA, Battaile KP, Lovell S, De Guzman RN. The crystal structures of the Salmonella type III secretion system tip protein SipD in complex with deoxycholate and chenodeoxycholate. Protein Sci. 2011; 20(1):75–86. [PubMed: 21031487]
29. Espina M, Ausar SF, Middaugh CR, Baxter MA, Picking WD, Picking WL. Conformational stability and differential structural analysis of LcrV, PcrV, BipD, and SipD from type III secretion systems. Protein Sci. 2007; 16(4):704–714. [PubMed: 17327391]
30. Lunelli M, Hurwitz R, Lambers J, Kolbe M. Crystal structure of PrgI-SipD: insight into a secretion competent state of the type three secretion system needle tip and its interaction with host ligands. PLoS Pathog. 2011; 7(8):e1002163. [PubMed: 21829362]
31. Prouty AM, Gunn JS. Salmonella enterica serovar typhimurium invasion is repressed in the presence of bile. Infect Immun. 2000; 68(12):6763–6769. [PubMed: 11083793]
32. Wang Y, Ouellette AN, Egan CW, Rathinavelan T, Im W, De Guzman RN. Differences in the electrostatic surfaces of the type III secretion needle proteins PrgI, BsaL, and MxiH. J Mol Biol. 2007; 371(5):1304–1314. [PubMed: 17617421]

33. Darboe N, Kenjale R, Picking WL, Picking WD, Middaugh CR. Physical characterization of MxiH and PrgI, the needle component of the type III secretion apparatus from Shigella and Salmonella. Protein Sci. 2006; 15(3):543–552. [PubMed: 16501225]

34. Kenjale R, Wilson J, Zenk SF, Saurya S, Picking WL, Picking WD, Blocker A. The needle component of the type III secreton of Shigella regulates the activity of the secretion apparatus. J Biol Chem. 2005; 280(52):42929–42937. [PubMed: 16227202]

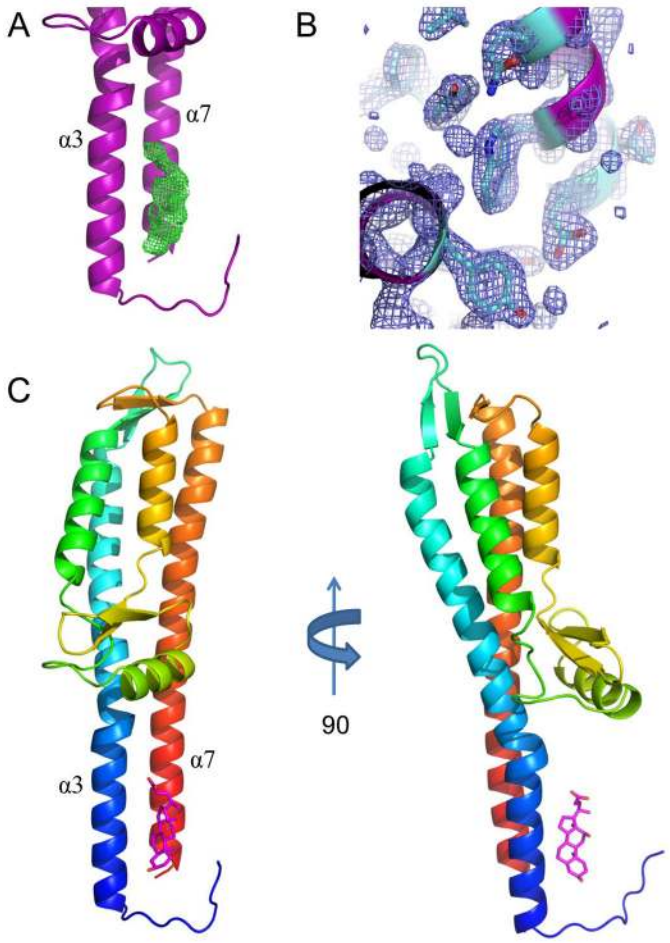

Figure 1. 1.90 Å-resolution cocrystal structure of IpaD$^{122.319}$ from *S. flexneri* bound to DOC

A, *Fo*–*Fc* map (green mesh at 2.0σ contour, carve radius of 1.6 Å) of the refined structure, following a single round of atomic-displacement factor and occupancy refinement in the absence of modeled bile salt in order to eliminate "phase memory bias". IpaD backbone is depicted in cartoon ribbon format (purple). *B*, Representative model-to-map correlation of an aromatic region of IpaD$^{122.319}$ with the *2Fo–Fc* weighted electron density (contoured at 2.0σ) depicted as a blue mesh. *C*, Crystal structure of a single copy of IpaD$^{122.319}$ in cartoon ribbon format bound to DOC. The two views of the molecule are related by a 90 degree rotation about the central coiled-coil axis. Molecule A is depicted in all three panels.

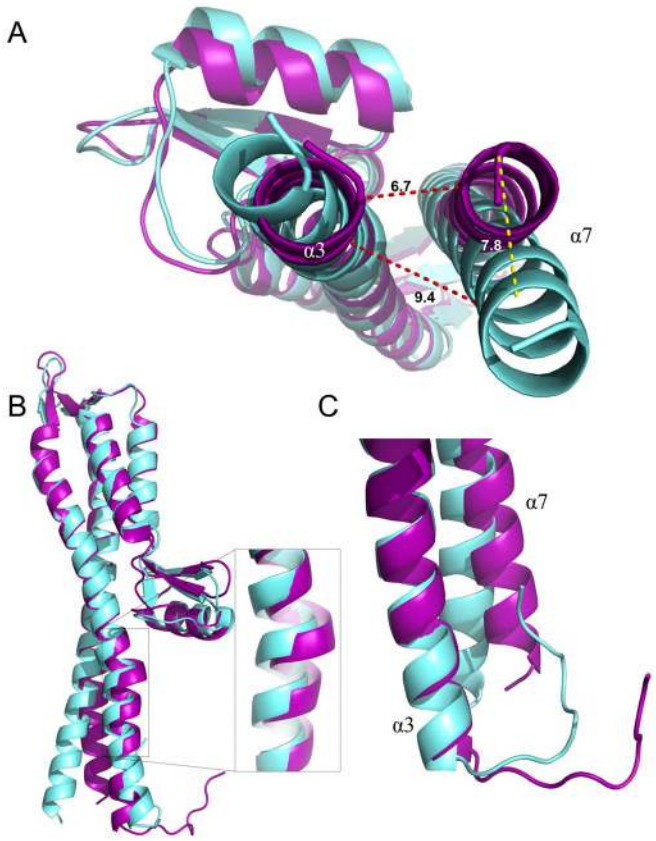

Figure 2. Structural superposition of free and DOC-bound IpaD crystal structures

PDB ID: 2J0O, 'free' IpaD$^{15–332}$ (aquamarine); 3R9V, DOC-bound IpaD$^{122.319}$ (purple). *A*, Structural superposition of free and DOC-bound IpaD structures. Constriction of α3 (left) and α7 (right) highlighted (in red) with distance apart (Å) for both structures (measured from Ile138 to Leu315 on each helix). Movement of α7 (measured from Thr319 carbonyl atom of each structure) within both structures is highlighted in yellow. *B*, Superposition of free and DOC-bound IpaD structures highlighting the exacerbation of the 'kink' region. Coloring of both structures is the same as in panel A. *C*, Superposition of free and DOC-bound IpaD structures, highlighting the distension of the 10 most N-terminal residues within the DOC-bound structure when compared to the equivalent region in free IpaD (DOC removed for clarity). Coloring of both structures is the same as in panel A.

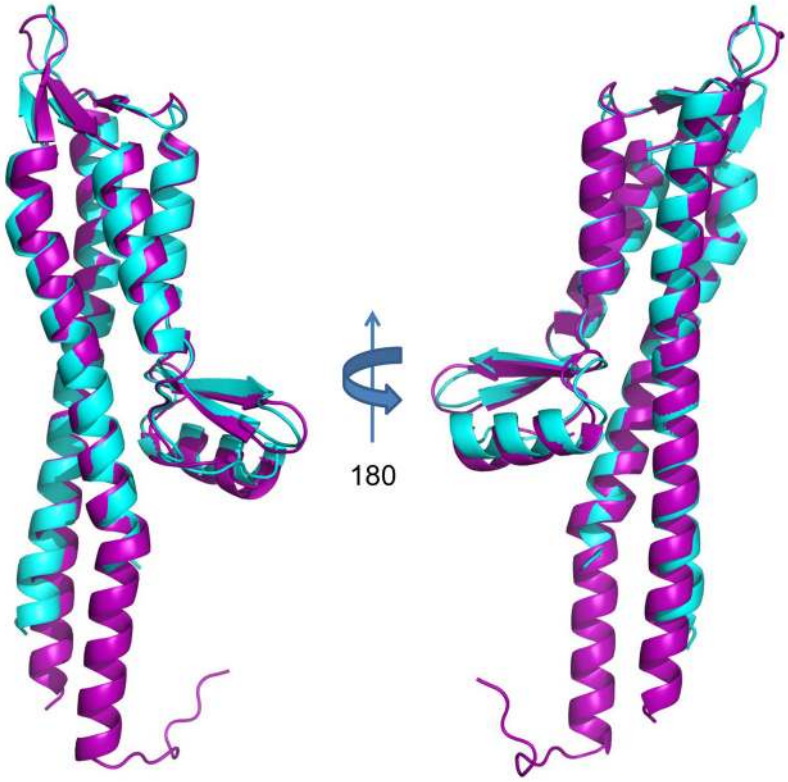

Figure 3. Structural superposition of truncated and DOC-bound IpaD crystal structures

Crystal structures of proteolytically truncated, free IpaD (PDB ID: 2J0N, chain A, colored cyan) and DOC-bound IpaD$^{122.319}$ (colored purple). 168/198 Cα positions align within 5.0 Å with an RMSD of 1.18 Å. The superpositioned structures are rotated 180° about the central coiled-coil axis on the right.

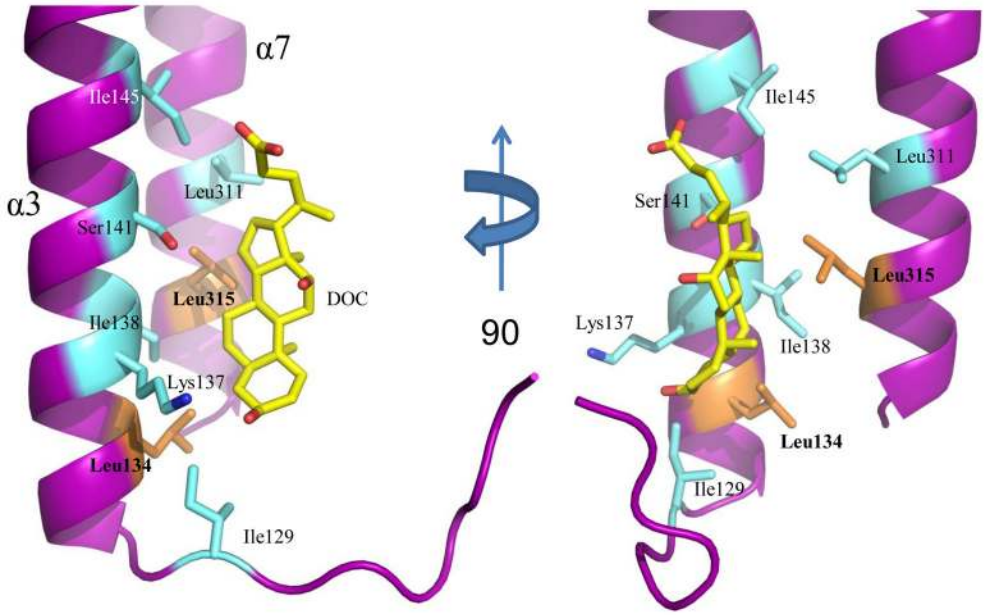

Figure 4. DOC-bound active site within IpaD

Amino acid side chains (aquamarine) of IpaD$^{122.319}$ within 2.6 – 5.0Å of DOC (yellow). IpaD backbone is depicted in cartoon ribbon format (purple). Side chains intimately involved in DOC interaction, Leu134 and Leu315, are highlighted in orange. Crystal structure rotated 90° about the central coiled-coil axis on the right.

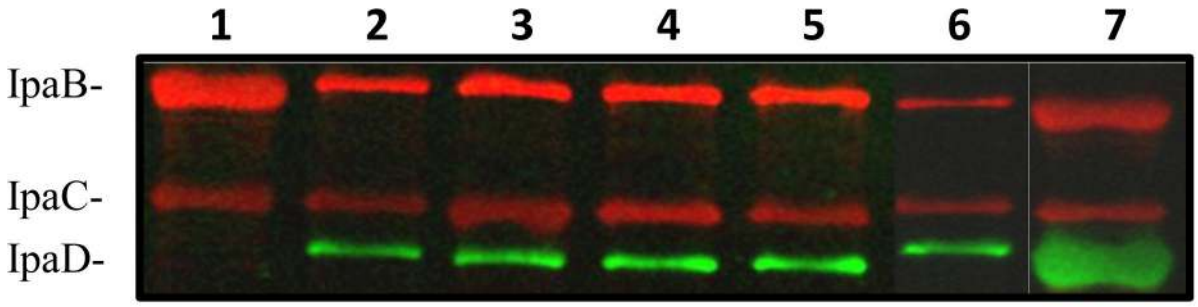

Figure 5. Control of overnight secretion for *S. flexneri* SF622 expressing different IpaD mutants

Bacteria were grown overnight in TSB and the proteins present in equal amounts of culture supernatant were separated by SDS-PAGE. IpaB, IpaC and IpaD (labeled) were then detected by immunoblot analysis as described in Methods. The relative abundance of each protein was estimated based on the size of the observed bands. The lanes shown are for supernatants from the following: 1) *S. flexneri* SF622 (*ipaD* null mutant), 2) SF622 expressing wild-type IpaD or 3) L134S, 4) K137S, 5) I138S, 6) L315S, and 7) L134S/ L315S. The level of overnight secretion seen for the complemented strain was similar to that seen for overnight secretion by wild-type *S. flenxeri* [11].

Table I

Bacterial strains used in the study

Strain designation	Resistance
Shigella flexneri ipaD null (SF622)	Kan
SF622 harboring pWPsf4D[a]	Amp/Kan
L134S[b]	Amp, Kan
L134E	Amp, Kan
K137S	Amp, Kan
I138S	Amp, Kan
L315S	Amp, Kan
L315E	Amp, Kan
L134S/L315S	Amp, Kan
L134E/L315E	Amp, Kan

[a] pWPsf4D contains the wild-type *ipaD* gene for expression in *S. flexneri*.

[b] Each mutant designation is for IpaD harboring the designated amino acid change encoded on pWPsf4.

Table II

Diffraction Data Collection and Structure Refinement Statistics

Data Collection[a]	
Crystal	IpaD-DOC
Beamline	APS 22-BM
Wavelength (Å)	1.0000
Space Group	$P2_1$
Cell Dimensions	a=62.97, b=43.72, c= 93.76 β=97.42°
Resolution (Å)	25.28-1.90 Å
Reflections (unique)	224,385 (39,374)
Completeness (%)	97.7 (82.9)
Redundancy (fold)	5.7
<I>/<σI>	21.1 (2.48)
R_{merge} (%)[b]	7.2 (45.1)
Refinement	
RCSB Accession Code	3R9V
Protein Molecules/AU	2
R_{work}/R_{free} (%)[c]	22.9/25.5
Number of Atoms	
Protein	2826
Ligand	56
Solvent	244
Ramachandran Plot (%)	
Favored	96.6
Allowed	2.3
Outliers	1.1
RMSD	
Bond Lengths (Å)	0.010
Bond Angles (°)	1.186
B factor (Å^2)	
Protein	38.0
Ligand	37.4
Solvent	38.8
Ligand Occupancy (%)	
Chain A	0.95
Chain B	0.96

[a] Numbers in parentheses are for the highest-resolution shell.

[b] $R_{merge} = \Sigma_h\Sigma_i|I_i(h)-\langle I(h)\rangle|/\Sigma_h\Sigma_i I_i(h)$, where $I_i(h)$ is the ith measurement of reflection h and $\langle I(h)\rangle$ is a weighted mean of all measurements of h.

[c] $R = \Sigma_h|F_{obs}(h)-F_{calc}(h)|/\Sigma_h|F_{obs}|$. R_{cryst} and R_{free} were calculated from the working and test reflection sets, respectively. The test set constituted 5% of the total reflections not used in refinement.

Table III

Site directed mutagenesis of key residues involved in DOC binding

IpaD form	Relative Invasion		Hemolysis (%)[c]		IpaD on Surface[d]	
	– DOC[a]	+ DOC[b]	−DOC	+DOC	−DOC	+DOC
Null	0	0	1.9	2.0	0	0
Wild-type	100	335	30.1	23.9	95	93
L134S	141	125	33.5	31.1	98	96
L134E	152	200	38.4	32.9	95	93
K137S	74	237	27.8	25.3	95	96
I138S	91	333	31.7	33.1	94	96
L315S	147	614	35.5	31.4	97	92
L315E	10	0	5.5	3.0	5	<5
L134S/L315S	0	0	1.4	2.0	0	0
L134E/L315E	0	0	1.8	1.7	0	0

[a] Relative to invasion by *S. flexneri* expression wild-type IpaD without DOC added. All invasion results are with less than 15% standard deviation for any individual experiment. Experiments were repeated at least three times. The activity of the complemented *S. flexneri* strain was approximately 80% as invasive as wild-type M90T [10]. The wild-type bacteria also responded to DOC with similarly enhanced invasiveness.

[b] Contact-mediated hemolysis is shown relative to complete hemolysis caused by the addition of water.

[c] Contact-mediated hemolysis was determined by a modification of our standard procedure. The number of bacteria and incubation time used were reduced and the values given are relative to 100% lysis using water. A PBS negative control for lysis had a value of 2.2% lysis and all values have a standard deviation of less than 2% based on triplicate measurements from multiple experiments.

[d] Surface localization of IpaD was determined by immunofluorescence staining using anti-IpaD antibodies and is given as the percent cells in multiple fields possessing visible IpaD on their surfaces. Results for L315E varied and in some cases there was no IpaD visible on the bacterial surface prior to addition of DOC.